Atomistic simulations incorporating nonlinear elasticity: Slow-stress relaxation and symmetry breaking

J. V. Lill and Jeremy Q. Broughton
Complex Systems Theory Branch, Code 6692, Naval Research Laboratory, Washington, D.C. 20375-5345
(Received 28 June 1993; revised manuscript received 6 December 1993)

Complementary molecular-dynamics and Metropolis Monte Carlo algorithms for the atomistic simulation of crystals with imposed laboratory conditions of temperature and tensorial pressure are presented. Inclusion of the *nonlinear* expression for the elastic energy of a crystal yields simulations that conserve the Gibbs potential of the crystal despite finite deformations. The molecular-dynamics equations of motion contain an explicit expression of the virial theorem for nonlinear elastic media; the dynamical balance of the "internal" and "external" pressures includes the elastic response of the system to the applied stress. Thus the "internal" and "external" pressures remain in dynamical equilibrium even when the microscopic dynamics generate a phase transformation and the initial isotropy of the macroscopic stress field is broken. Deterministic molecular-dynamics trajectories for a simple pair-potential model of a pressure-induced martensitic transformation are presented; manifestly nonlinear behavior is observed while satisfying the tensorial virial theorem for nonlinear elastic media. Stochastic Monte Carlo trajectories yield comparable results, and independently verify the nonlinear extension of the virial theorem. This is despite the fact that the Monte Carlo algorithm contains no explicit driving terms that insure the theorem be satisfied.

I. INTRODUCTION

The standard definitions of enthalpy and Gibbs free energy of an elastic medium differ from those of a liquid (which are more familiar, perhaps, to the atomistic community) in that a reference lattice is required from which the strain is measured. The modern continuum literature has been concerned with what happens during a phase transition—e.g., a martensitic transition—since the reference lattice clearly imparts a history dependence to the system. Continuum practitioners consider issues such as daughter phases imbedded in parent phases. The atomistic community, on the other hand, has largely concerned itself with describing phase transitions in which the entire periodic system converts simultaneously to the new phase. The true state of affairs in a given system lies somewhere between these two extremes. As the computational volume in an atomistic simulation undergoes its transition (the daughter phase) stress develops which will and must relax at some rate. The limit of *infinitely slow* stress relaxation (on an atomic time scale) is the subject of the present paper. We seek to bring atomistic and continuum descriptions rigorously into line. History dependence is therefore incurred by necessity. In a subsequent paper, we describe how to effect stress relaxation on a finite time scale, thereby relating the linear and nonlinear methods. The former is closer to that which prevails in phase transitions of liquids, for example, in which relaxation times are fast; but even here, a method incorporating an albeit fast but finite time relaxation is more realistic.

When incorporated into atomistic simulations in a rigorous manner, linear and nonlinear elastic reservoirs interact with the atomic system in qualitatively different manners. In both cases, the elastic reservoirs can affect the behavior of the atoms; however, only in the nonlinear case can the atoms affect the behavior of the reservoir as well. It is this quality that will allow us to simulate the change in stress imposed on the daughter phase as it transforms, and which serves as a signature for the symmetry breaking inherent in such processes. The internal and effective external stresses on the daughter phase remain in dynamic equilibrium even though the change in symmetry can lift degeneracies, etc., in the tensorial values of these quantities. If stress relaxation is allowed over some finite time interval, then the system loses all memory of the original reference lattice and of the symmetry breaking during the transition. These effects can have a profound influence on the development of the phase transition. For example, the strain induced by the parent crystal on the daughter phase is thought to be crucial to the subsequent microscopic structure. In this paper we consider only nonlinear methods in the limit of a long relaxation time.

The use of deterministic molecular-dynamics (MD) trajectories to simulate an isobaric ensemble originated with Andersen.[1] In his method the simulation volume became a dynamical variable. The rigor of the method arises from the demonstration that the trajectories sample the correct distribution function, assuming ergodicity. Parrinello and Rahman[2–4] quickly generalized this approach to include deformations of the simulation volume; the lattice vectors describing the shape of the simulation volume became dynamical variables. First the scalar pressure,[2,3] and later the tensorial pressure,[4] was controlled in this manner. Shortly thereafter, Nosé[5–7] demonstrated how to control temperature deterministically by using a time scale as a dynamical variable. Hoover[8] simplified this approach through the introduction of a generalized friction, that could either add to or subtract from the atomic velocities. He also noted that the

dynamics of the time scale became decoupled from those of the remaining degrees of freedom, and wrote the equations governing the atomic motion in the physical rather than the virtual time. We have chosen to formulate our equations in physical time using Hoover's friction, but with the atomic coordinates and momenta scaled by the lattice vectors. A brief discussion of other possibilities will be given later.

Modifications of the original Parrinello-Rahman dynamics were suggested by Ray and Rahman[9,10] and Ray.[11] Their main point was to change the definition of the *strain energy* used in the derivation of Parrinello and Rahman[4] to the nonlinear expression[12] used in continuum theory. We have reconsidered the incorporation of nonlinear elastic effects into atomistic simulations and have obtained qualitatively different results from the linear theory of Parrinello and Rahman,[2–4] and the original nonlinear analysis of Ray and Rahman.[9,10] A preliminary report of this work has appeared;[13] we here present the results in more detail. Algorithmic details may be found elsewhere.[14]

The principle mathematical result of this work is a set of dynamical equations governing the shape of the simulation cell; the main physical result is an interpretation of these dynamical equations in terms of the tensorial virial theorem[15] as applied to nonlinear elastic media. We also present a dynamical constraint to eliminate rigid rotations of the simulation cell, that is distinct from the original geometrical constraint of Nosé and Klein.[16] Further, we guarantee that our equations of motion are formally invariant to the arbitrary choice of lattice vectors, as discussed by Cleveland[17] and by Wentzcovitch.[18] Finally, we have referred the dynamics of the simulation volume to a set of vectors used to span the volume.

By way of corroboration, we have also constructed a Metropolis Monte Carlo (MC) algorithm[19] to sample the same distribution function as that of the MD algorithm. There is no special biasing in this MC algorithm which insures satisfaction of the nonlinear tensorial virial theorem, and the algorithm is free from any dynamical considerations that give rise to the differences between our MD algorithm and previous linear[4] and nonlinear[10] methods. Agreement between our MD and MC results thus confirms that the nonlinear behavior exhibited is due to the physics as dictated by the underlying distribution function. We have found it convenient to extend the standard Metropolis procedure to include "movements" of atomic momenta. This is analogous to Andersen's hybrid MD-MC method to control temperature, but we "move" all momenta at once, drawing uncorrelated variates directly from the correct distribution. These kinetic effects appear in the Boltzmann factors for deformations of the simulation cell.

The present analysis is restricted to *homogeneous* deformations, but one must be very careful in defining precisely what this means. We do not constrain every atom to follow (on average) the motion of the single set of lattice vectors which span the simulation cell, and formally the only periodicity imposed is that of the simulation cell itself. This restriction to a single set of lattice vectors, and hence to homogeneous deformations, is shared with previous linear[2–4] and nonlinear[9,10] MD methods; however, our nonlinear analysis differs qualitatively from these through the introduction of memory effects. Within the homogeneous treatment of structural phase transformations, memory effects arise from the retention of a single reference lattice, and model the strain induced in the parent crystal from the inclusion of islands of the new structural phase. This physical interpretation is made clear mathematically through satisfaction of the nonlinear tensorial virial theorem. Stated simply, this insures that the internal pressure of the simulation cell, as dictated by the interatomic potential, balances the external pressure, as dictated by the imposed laboratory conditions and the elastic response of the crystal to these conditions.

The outline of the paper is as follows: In Sec. II we establish some necessary notation and discuss differences between the linear and nonlinear expressions for the strain energy. In Sec. III we present the MC algorithm; in Sec. IV we derive the MD equations of motion. Numerical results of MD and MC simulations are compared in Sec. V. A discussion follows in Sec. VI.

II. DEFORMATIONS AND STRAIN ENERGY

We employ a simple matrix notation with a summation convention for repeated indices to describe Cartesian tensors. An arbitrary crystal may be described by three lattice vectors arranged in a 3×3 matrix where $\mathbf{a}_{ij}$ is the ith Cartesian component of the jth crystalline lattice vector. We use $\mathbf{a}_{ij}$ to denote a particular element of the matrix of crystalline lattice vectors, or the matrix itself:

$$\mathbf{a}_{ij}=\begin{pmatrix}\mathbf{a}_{x1} & \mathbf{a}_{x2} & \mathbf{a}_{x3}\\ \mathbf{a}_{y1} & \mathbf{a}_{y2} & \mathbf{a}_{y3}\\ \mathbf{a}_{z1} & \mathbf{a}_{z2} & \mathbf{a}_{z3}\end{pmatrix}. \tag{2.1}$$

The first index of any matrix always refers to the row, and the second index to the column. Thus the row space of $\mathbf{a}_{ij}$ is labeled by the Cartesian coordinates and the column space of $\mathbf{a}_{ij}$ is labeled by the *arbitrary* set of lattice vectors used to describe the crystal; the row and column spaces of other matrices may be determined by the context in which they appear. $\mathbf{a}_{ij}$ is the dynamic lattice; in MD simulations it is time dependent, while in MC simulations it is subject to stochastic deformations. Similarly, we define the matrix of reference lattice vectors as $\mathbf{b}_{ij}$, whose elements remain constant during simulations. The presence of the reference lattice is required by the nonlinear theory of elasticity. For brevity we say that $\mathbf{a}_{ij}$ is the *dynamic* lattice and $\mathbf{b}_{ij}$ is the *reference* lattice. The lattice vectors $\mathbf{a}_{ij}$ can describe either primitive or unit cells of an arbitrary crystal, i.e., the smallest cells capable of spanning the crystal, or those cells possessing all the symmetries of the crystallographic point group.[22] To avoid confusion, we use the term "crystalline cell" to include all possibilities. We need not consider the basis vectors that specify atomic positions within the crystalline cell here.

In order to impose thermodynamic conditions of con-

stant stress, we follow Ray and Rahman[9,10] and define scaled atomic positions and momenta by

$$\mathbf{r}_i^{(n)}=\mathbf{a}_{ij}\mathbf{q}_j^{(n)} \Longleftrightarrow \mathbf{q}_i^{(n)}=\mathbf{a}_{ij}^{-1}\mathbf{r}_j^{(n)} , \tag{2.2}$$

and

$$\mathbf{p}_i^{(n)}=\mathbf{a}_{ji}^{-1}\pi_j^{(n)} \Longleftrightarrow \pi_i^{(n)}=\mathbf{a}_{ji}\mathbf{p}_j^{(n)} , \tag{2.3}$$

where $\mathbf{r}_i^{(n)}$ and $\mathbf{p}_i^{(n)}$ are the positions and momenta of atom n in the Cartesian coordinates, and $\mathbf{q}_i^{(n)}$ and $\pi_i^{(n)}$ are the corresponding scaled quantities. By $\mathbf{a}_{ij}^{-1}$ we mean the element of the ith row and jth column of the inverse of the matrix of lattice vectors. Interatomic distances may be computed using the scaled coordinates as

$$r_{nm}=\sqrt{(\mathbf{q}_i^{(n)}-\mathbf{q}_i^{(m)})\mathbf{g}_{ij}(\mathbf{q}_j^{(n)}-\mathbf{q}_j^{(m)})} , \tag{2.4}$$

where the metric is

$$\mathbf{g}_{ij}=\mathbf{a}_{ki}\mathbf{a}_{kj} . \tag{2.5}$$

This equation reads: "The metric equals the transpose of the matrix of lattice vectors times the matrix of lattice vectors."

In the dynamical equations that follow, it will become apparent that this scaling allows us to treat $\mathbf{a}_{ij}$ as describing a *macroscopic* crystal. Specifically, the atoms in the simulation will not be constrained to strictly follow deformation of $\mathbf{a}_{ij}$ in the homogeneous fashion discussed by Born and Huang.[20] Strictly speaking, Born and Huang defined two types of atoms, those whose positions were specified only by the lattice vectors, and those whose positions required additional basis vectors. The former atoms deform homogeneously, while the latter may deform nonhomogeneously, thus giving rise to two distinct terms in the strain energy, the "Born" and "relaxation" terms. We adopt a more general point of view here where the atoms are not explicitly constrained, and where the elastic properties of the material are determined by the average atomic behavior throughout the entire simulation cell spanned by the vectors $\mathbf{a}_{ij}$.

The transformation connecting the reference lattice to the dynamic lattice is the deformation gradient $\mathbf{J}_{ij}$,

$$\mathbf{J}_{ij}=\mathbf{a}_{ik}\mathbf{b}_{kj}^{-1} . \tag{2.6}$$

We consider homogeneous deformations of $\mathbf{a}_{ij}$ in the macroscopic sense, i.e., the deformation gradient is assumed to have translational invariance throughout. Suitably invariant measures of the strain dating back to Cauchy are then[12,21]

$$\eta_{ij}=\tfrac{1}{2}(\mathbf{J}_{ki}\mathbf{J}_{kj}-\delta_{ij}) , \tag{2.7}$$

or

$$\mu_{ij}=\tfrac{1}{2}(\delta_{ij}-\mathbf{J}_{ki}^{-1}\mathbf{J}_{kj}^{-1}) , \tag{2.8}$$

where δ_{ij} is the Kronecker symbol.

Coordinate rotations may be effected through application of the Euler rotation matrix $\mathbf{E}_{ij}$ as

$$\mathbf{J}'_{ij}=\mathbf{E}_{im}\mathbf{J}_{mn}\mathbf{E}_{jn} , \tag{2.9}$$

for example. Here $\mathbf{J}'_{ij}$ is the deformation gradient in the rotated frame. This transformation is seen to be equivalent to a rigid rotation of the crystal. Another distinct transformation corresponds to making a different choice for the lattice vectors used to describe the crystal. This may be effected through application of the modular transformation $\mathbf{M}_{kj}$,

$$\mathbf{a}^*_{ij}=\mathbf{a}_{ik}\mathbf{M}_{kj} , \tag{2.10}$$

where $\mathbf{M}_{kj}$ is a matrix of integers with a unit determinant,

$$|\mathbf{M}|=1 , \tag{2.11}$$

and where the elements of $\mathbf{a}^*_{ij}$ are the components of the new lattice vectors. We must similarly transform the reference lattice vectors as

$$\mathbf{b}^*_{ij}=\mathbf{b}_{ik}\mathbf{M}_{kj} , \tag{2.12}$$

etc. Note that the deformation gradient is invariant to modular transformations. We will make our MD equations formally invariant to the choice of lattice vectors through use of the elements of the deformation gradient as the independent variables. This is the nonlinear extension of the original linear proposal of Wentzcovitch.[18]

The nonlinear expression for the strain energy is given by[12]

$$\Phi_{\text{strain}}=|\mathbf{b}|(\tau_{ij}\eta_{ij})=|\mathbf{a}|(\sigma_{ij}\mu_{ij}) , \tag{2.13}$$

where the stress σ_{ij} and the thermodynamic tension τ_{ij} are related by

$$\tau_{ij}=|\mathbf{J}|(\mathbf{J}_{ik}^{-1}\sigma_{kl}\mathbf{J}_{jl}^{-1}) . \tag{2.14}$$

This expression is invariant to both coordinate rotations and to modular transformations. The expressions in (2.13) are seen to represent the trace of the product of two symmetric matrices. It is σ_{ij}, the stress that would occur in the crystal in the absence of any deformation, that will be specified in the simulations to follow.

Connection with the linear theory is obtained through consideration of an infinitesimal deformation (ε_{ij}) of the reference lattice

$$\mathbf{J}_{ij}\approx(\delta_{ij}+\varepsilon_{ij}) .$$

The linear approximation for the strain energy is then

$$\Phi_{\text{strain}}\approx|\mathbf{a}|(\sigma_{ij}\bar{\varepsilon}_{ij}) , \tag{2.15}$$

where the symmetrized infinitesimal strain,

$$\bar{\varepsilon}_{ij}=\tfrac{1}{2}(\varepsilon_{ij}+\varepsilon_{ji}) , \tag{2.16}$$

insures that rigid rotations of the crystal are eliminated from its thermodynamic description.[12] The elimination of the energy associated with rigid rotations of a crystal from its thermodynamical potential—or more generally, from its constitutive equation—is in accordance with the *principle of material-frame indifference.*[21] We will insure that rigid rotations of our crystal are eliminated from the MD simulation through adherence to this condition dynamically at each instant of time.

It is seen that the linear and nonlinear expressions for

the strain energy can yield different results when finite deformations of the reference lattice are considered. In accordance with the *principle of fading memory,*[21] the entire history of a solid need not be known to describe its current condition. Thus, in a macroscopic phenomenological sense, experience dictates that the reference lattice relaxes to some equilibrium given sufficient time. This distinction gives rise to differences in the standard expressions for the Gibbs potential of an elastic crystal and that of a fluid.[12] These definitions are based on the different idealized constitutive assumptions that the crystal possesses a complete memory of its initial shape and a fluid possesses no such memory at all.

There are situations where each idealized assumption appears valid. Consider the following possibilities: If the entire macroscopic crystal undergoes a homogeneous phase transformation at once, the crystal simply becomes a new material having no memory of its initial shape. Such conditions are often realized when a small crystal is suspended in a fluid in a diamond anvil cell. The surrounding fluid relaxes immediately upon the crystal undergoing a phase transformation, and atomistic simulations based on linear elastic theory seem adequate. Conversely, if only a small portion of the crystal deforms, then the inclusion of the new phase in the parent crystal experiences the strain field of the original crystal; i.e., the new phase has some memory of its initial shape. Performance of atomistic simulations using the nonlinear methods presented here is then necessitated.

The inclusion of a new structural phase in the parent crystal and the relaxation of the resulting strain has been the subject of continuum models.[22] The atomistic methods to be presented here are similar in spirit but distinct from the continuum models based on what Khachaturyan calls the "homogeneous moduli approximation," as outlined in the diagram on p. 202 of Ref. 22. In particular, we do not make any suppositions concerning the elastic moduli of the parent and daughter phases; these are completely dictated by the interatomic potential and geometry of each phase. What is lacking in present methods (including that presented here) is any atomistic description of the boundary between the two phases, and any explicit method for relaxation of the strain induced in the parent crystal by inclusion of the new phase. Within the homogeneous approximation used here, any boundary effects are modeled by the retention of a single reference lattice and the resulting strain induced by the phase transformation. We now consider the specific ensemble to be sampled and a corresponding MC algorithm.

III. MONTE CARLO SIMULATIONS IN THE ISOTHERMAL-ISOSTRESS ENSEMBLE

Ray and Rahman[9,10] used the definition of the Gibbs potential of Thurston[12] to derive an expression for the partition function appropriate for the isothermal-isostress ensemble. Our expression differs from theirs only in the use of the deformation gradient instead of the matrix of lattice vectors and in the explicit expression of the constraints to exclude center-of-mass motion and rigid rotations:

$$\Xi_{N\sigma T}=\frac{1}{N!h_P^{3N}}\int d\mathbf{q}\int_{\mathrm{CM}}d\pi\int_{NR}d\mathbf{J}\exp\left[\frac{-1}{k_BT}[h\{\mathbf{q}_i^{(n)},\pi_i^{(n)};\mathbf{J}_{ij}\}-(N_{\mathrm{cells}}|\mathbf{b}|\tau_{ij}\eta_{ij})]\right]. \tag{3.1}$$

N is the number of atoms in the crystal, h_P is Planck's constant, k_B is Boltzmann's constant, and the atomic Hamiltonian is written as

$$h\{\mathbf{q}_i^{(n)},\pi_i^{(n)};\mathbf{J}_{ij}\}=\sum_{n=1}^{N}(\pi_i^{(n)}\mathbf{g}_{ij}^{-1}\pi_j^{(n)}/2\mu_n)+\Phi\{r_{nm}\}\ , \tag{3.2}$$

where μ_n is the mass of atom n. $\Phi\{r_{nm}\}$ denotes the interatomic potential energy, and is dependent on all the interatomic distances such as (2.4). We include the deformation gradient in (3.2) to indicate the dependence of the atomic Hamiltonian on the lattice vectors through the metric, both explicitly in (3.2) and implicitly through (2.4). The notation in (3.1) implies integration over each matrix element of the deformation gradient, and over all the atomic coordinates and momenta. We have chosen the elements of the deformation gradient as "coordinates" to describe the deformation of the computational cell, assuming that N_{cells} such fluctuating crystalline cells span the simulation volume as

$$N_{\mathrm{cells}}|\mathbf{a}|=V_{\mathrm{simulation}}\ . \tag{3.3}$$

The N_{cells} cells are assumed to contain a total of N atoms. We have also indicated the presence of dynamical constraints; the subscript "CM" implies that the atomistic system is constrained to have no center-of-mass momentum, and the subscript "NR" implies that the trajectories of the deformation gradient do not sample any phase space corresponding to a rigid rotation of the crystal. We consider three types of transitions between states labeled by k' and k, and having probability densities $\rho(k)$ and $\rho(k')$. The entire MC algorithm is summarized in Table I.

(1) First let k' and k denote points in phase space corresponding to states in which the scaled coordinates of one atom have been changed, leaving all the other atomic coordinates, momenta, and the strain of the cell unaltered. The symmetric underlying transition probability density matrix, $\mathbf{A}(\mathbf{q}_j'^{(n)}\leftarrow\mathbf{q}_j^{(n)})$ is a uniform distribution centered on zero, with a maximum allowed scaled atomic displacement of $\delta\langle q\rangle_{\max}$. The trial components of the

coordinates of atom n are then obtained by drawing a variate from this distribution, as denoted by $\chi\{\mathbf{A}(\mathbf{q}_j'^{(n)}\leftarrow\mathbf{q}_j^{(n)})\}$. The cost function then takes the simple form displayed in Table I, and the Boltzmann factors are computed as usual. Here all the interatomic distances affected by the change of the atom coordinates of atom n must be computed to obtain the change in the total potential energy due to the trial atomic translation.

(2) Next consider an infinitesimal stochastic deformation of the dynamic lattice. Again, the symmetric underlying transition probability density matrix is chosen to be a uniform density $\mathbf{A}(\eta_{ij}'\leftarrow\eta_{ij})$, this time in strain space. A stochastic infinitesimal strain is the 3×3 matrix of variates drawn from this density as in Table I. The stochastic infinitesimal strain is then symmetrized to remove rotations from the thermodynamic description of the crystal: the trial deformation gradient and corresponding trial values for all the geometrical tensors are denoted with primes in Table I. The resulting cost function then includes contributions from all the possible terms, and includes effects of the kinetic energy of the atoms because of the charge in the metric. Trial deformations are computationally costly, as the total atomic potential (rather than just the change in the total atomic potential) must be computed. We therefore perform many (e.g., several thousand) trial atomic translations between trial deformations.

(3) Typically, isothermal-isobaric MC simulations[23] are conducted exclusively in configuration space. This suppresses all physical fluctuations in the kinetic temper-

TABLE I. The MC algorithm.

Transition probability density matrix:

$$\mathbf{W}(k'\leftarrow k)=\begin{cases}\mathbf{A}(k'\leftarrow k)\ , & \rho(k')\geq\rho(k)\\ \mathbf{A}(k'\leftarrow k)\exp[\Theta(k'\leftarrow k)]\ , & \rho(k')<\rho(k)\end{cases}$$

Cost function for k to k' transition:

$$\Theta(k'\leftarrow k)=\left[\sum_{n=1}^{N}(\pi_i^{(n)}\mathbf{g}_{ij}^{-1}\pi_j^{(n)}/2\mu_n)+\Phi\{r_{nm}\}-(N_{\text{cells}}|\mathbf{b}|\tau_{ij}\eta_{ij})\right]_{k'}-\left[\sum_{n=1}^{N}(\pi_i^{(n)}\mathbf{g}_{ij}^{-1}\pi_j^{(n)}/2\mu_n)+\Phi\{r_{nm}\}-(N_{\text{cells}}|\mathbf{b}|\tau_{ij}\eta_{ij})\right]_{k}$$

Case 1, single atomic moves:

$$\mathbf{A}(\mathbf{q}_j'^{(n)}\leftarrow\mathbf{q}_j^{(n)})=\frac{1}{\delta\langle q\rangle_{\max}}\ ;\quad -\frac{\delta\langle q\rangle_{\max}}{2}\leq\delta\langle q\rangle\leq\frac{\delta\langle q\rangle_{\max}}{2}$$

$$\mathbf{q}_j'^{(n)}=\mathbf{q}_j^{(n)}+\chi\{\mathbf{A}(\mathbf{q}_j'^{(n)}\leftarrow\mathbf{q}_j^{(n)})\}$$

$$\Theta(\mathbf{q}_j'^{(n)}\leftarrow\mathbf{q}_j^{(n)})=[\Phi\{r_{nm}\}]_{k'}-[\Phi\{r_{nm}\}]_k$$

Case 2, deformation of crystal:

$$\mathbf{A}(\eta_{ij}'\leftarrow\eta_{ij})=\frac{1}{\delta\langle\eta\rangle_{\max}}\ ;\quad -\frac{\delta\langle\eta\rangle_{\max}}{2}\leq\delta\langle\eta\rangle\leq\frac{\delta\langle\eta\rangle_{\max}}{2}$$

$$\varepsilon_{ij}=\chi\{\mathbf{A}(\eta_{ij}'\leftarrow\eta_{ij})\}\ ,\quad \bar{\varepsilon}_{ij}=\tfrac{1}{2}(\varepsilon_{ij}+\varepsilon_{ji})$$

$$\mathbf{J}_{ij}'=(\delta_{ik}+\bar{\varepsilon}_{ik})\mathbf{J}_{kj}\ ,\quad \eta_{ij}'=\tfrac{1}{2}(\delta_{ij}+\mathbf{J}_{ki}'\mathbf{J}_{kj}'),\ \text{etc.}$$

$$r_{nm}'=\sqrt{(\mathbf{q}_i^{(n)}-\mathbf{q}_i^{(m)})\mathbf{g}_{ij}'(\mathbf{q}_j^{(n)}-\mathbf{q}_j^{(m)})}$$

$$\Theta(\eta_{ij}'\leftarrow\eta_{ij})=\left[\sum_{n=1}^{N}(\pi_i^{(n)}\mathbf{g}_{ij}'^{-1}\pi_j^{(n)}/2\mu_n)+\Phi\{r_{nm}'\}-(N_{\text{cells}}|\mathbf{b}|\tau_{ij}'\eta_{ij}')\right]_{k'}-\left[\sum_{n=1}^{N}(\pi_i^{(n)}\mathbf{g}_{ij}^{-1}\pi_j^{(n)}/2\mu_n)+\Phi\{r_{nm}\}-(N_{\text{cells}}|\mathbf{b}|\tau_{ij}\eta_{ij})\right]_{k}$$

Case 3, generation of new atomic momenta:

$$\mathbf{A}(\mathbf{p}_i^{(n)})=\frac{1}{2\pi\sqrt{\mu_n k_B T}}\exp\{-[\mathbf{p}_k^{(n)}\mathbf{p}_k^{(n)}/2\mu_n k_B T]\}$$

$$\mathbf{p}_j^{(n)}=\chi\{\mathbf{A}(\mathbf{p}_i^{(n)})\}\ ,\quad \pi_i^{(n)}=\mathbf{a}_{ji}\mathbf{p}_j^{(n)}$$

ature. In principle, such fluctuations can be integrated out of equilibrium ensemble averages, but we have found it convenient to include such fluctuations by specifying trial sets of "thermalized" atomic momenta every time a stochastic deformation is attempted. We employ mass-normalized Gaussian probability densities for each atomic species, compute the Cartesian trial components of the atomic momenta by drawing variates from these densities, and then compute the scaled atomic momenta using the current (not the trial) matrix of lattice vectors. The new scaled momenta can then be substituted into the cost function. This is essentially the same procedure used to initialize the atomic momenta for a MD simulation, and is rapid because no forces must be computed. We can generate new sets of thermalized atomic momenta, drawing variates directly from the appropriate Gaussian distributions and eliminating center-of-mass momentum, with no need for any Markov chain *per se* to find the appropriately distributed points in momentum space. We can move all the atomic momenta at once by drawing the variates directly from the Gaussian distributions for each type of atom, and no such move is ever rejected.

These methods are distinct from previous MC algorithms used to simulate uniaxial loading[24] through our incorporation of the nonlinear theory and appropriate invariance principles, and in the generality of the stresses and geometries that can be considered. We now proceed to derive MD equations of motion to sample the same distribution.

IV. MOLECULAR-DYNAMICS SIMULATIONS IN THE ISOTHERMAL-ISOSTRESS ENSEMBLE

The procedure employed here to generate MD equations of motion appropriate for the isothermal-isostress ensemble differs only slightly from that of previous analyses.[1-11] We begin with the extended virtual Hamiltonian[10,11] including scaling variables

$$h' = \sum_{n=1}^{N} (\pi_i'^{(n)} \mathbf{g}_{ij}^{-1} \pi_j'^{(n)} / 2\mu_n s^2) + \Phi\{r_{nm}\} + \frac{\theta^2}{2Q} + (f k_B T)\ln(s) + N_{\text{cells}} \left[\frac{1}{2W} \Omega_{ij}' \Omega_{ij}' / s^2 - |\mathbf{b}| \tau_{ij} \eta_{ij} \right] . \quad (4.1)$$

Here t is the physical time and t' is the virtual time; this notation is reversed from that used by Nosé.[6] These times are related through the time scale s by

$$\frac{\partial}{\partial t'} = \frac{1}{s} \frac{\partial}{\partial t} \Longleftrightarrow dt' = s\, dt . \quad (4.2)$$

The momentum canonically conjugate to s is θ. We have chosen not to scale this momentum with s for convenience.[25] However, we have chosen to so scale both the atomic momenta $\pi_i^{(n)}$ and cell momenta Ω_{ij}, i.e.,

$$\pi_i'^{(n)} / s = \pi_i^{(n)} \quad (4.3)$$

and

$$\Omega_{ij}' / s = \Omega_{ij} . \quad (4.4)$$

This is motivated by our interest in large and *rapid* deformations. Nosé[7] demonstrated that degrees of freedom having disparate time scales could be thermostated at different temperatures; here we consider the opposite case and employ a single time scale to describe rapid deformations. Equations (4.3) and (4.4) then imply that the deformation of the crystal can occur on the same time scale as the atomic motion. We specify the matrix elements of the deformation gradient, $\mathbf{J}_{ij}$, as the independent coordinates to describe the lattice dynamics; the matrix elements of $[N_{\text{cells}} \Omega_{ij}']$ are then the scaled canonically conjugate momenta. The use of the deformation gradient insures that the extended virtual Hamiltonian is formally invariant to modular transformations, and the inclusion of the factor N_{cells} refers all strain energies, etc., to the volume of the crystalline cell. The effective masses Q and W in (4.1) describe fluctuations of the temperature and the pressure of the system, respectively. Finally, f is the number of degrees of freedom and must be determined after all constraints have been imposed.

Following Nosé,[6] the equations of motion in physical time are displayed in Table II. Although noncanonical in form, these equations rigorously conserve the extended Hamiltonian h', (4.1). The transformation to physical time introduces a friction[8] into the atomic and lattice dynamics. Equation (T7) is the principle new result of this analysis. $\mathbf{P}_{kq}$ is the typical internal virial pressure, and Π_{kq} is a tensor we call the effective external pressure.

Because one can derive thermostated molecular dynamics using either Hamiltonian or Lagrangian formalisms, and write the results in either scaled or Cartesian coordinates, the resulting equations of motion can assume a number of seemingly different forms. This is particularly true for the equations governing atomic motion when the computational cell can deform. In particular, Ciccotti and Ryckaert[26] have presented MD equations for molecular systems using Cartesian atomic coordinates and accelerations, while Melchionna, Ciccotti, and Holian[27] extended Hoover's original work[8] to derive linear isothermal-isobaric equations using Cartesian atomic coordinates and momenta (see Ref. 28 for a recent review). For comparison, apparently different atomic equations of motion which are in fact equivalent to those presented here and earlier[13] are summarized in Table III; these are all related through straightforward transformations. More recently, Kusnezov and co-workers have presented more general equations of motion that include two independent frictional variables.[29,30] The resulting atomic equations are distinct from those presented here. As noted by Bylander and Kleinman,[31] the center-of-mass motion must be removed from the dynamics for a meaningful application of the Nosé temperature control. While all the atomic equations of motion in Table III are equivalent, the nonlinearity in the equations governing the pressure in Table II are unique to our method.

Use of either Lagrangian or Hamiltonian formalisms is a matter of taste; Ciccotti and Ryckaert[26] discuss the advantages of the use of Cartesian coordinates in formulating constraint algorithms for the simulation of molecular

TABLE II. The MD algorithm.

$$\dot{s}=\xi s \tag{T1}$$

$$\dot{\xi}=\frac{1}{Q}\left[\sum_{n=1}^{N}(\pi_i^{(n)}\mathbf{g}_{ij}^{-1}\pi_j^{(n)}/\mu_n)+\frac{N_{\text{cells}}}{W}\Omega_{ij}\Omega_{ij}-(fk_BT)\right] \tag{T2}$$

$$f=3N+3 \text{ (physical time averages, no center-of-mass motion, no rigid rotations)} \tag{T3}$$

$$\dot{\mathbf{q}}_i^{(n)}=\mathbf{g}_{ij}^{-1}\pi_j^{(n)}/\mu_n \tag{T4}$$

$$\dot{\pi}_i^{(n)}=\sum_{m=1}^{N;m\neq n}\left[\frac{-1}{r_{nm}}\frac{\partial\phi_{nm}}{\partial r_{nm}}\right]\mathbf{g}_{ij}(\mathbf{q}_j^{(n)}-\mathbf{q}_j^{(m)})-\xi\pi_i^{(n)} \tag{T5}$$

$$\dot{\mathbf{J}}_{ij}=\frac{1}{W}\Omega_{ij} \tag{T6}$$

$$\dot{\Omega}_{kp}=(\mathbf{P}_{kq}-\Pi_{kq})|\mathbf{a}|\mathbf{J}_{pq}^{-1}-\xi\Omega_{kp} \tag{T7}$$

$$\Omega_{ij}^{s}=\tfrac{1}{2}[\Omega_{ip}\mathbf{J}_{pk}^{-1}+\Omega_{kp}\mathbf{J}_{pi}^{-1}]\mathbf{J}_{kj} \tag{T8}$$

$$\begin{aligned}\mathbf{P}_{ij}=&\left[\sum_{n=1}^{N}(\mathbf{p}_i^{(n)}\mathbf{p}_j^{(n)}/\mu_n)\right](V_{\text{simulation}})^{-1}\\&+\left[\tfrac{1}{2}\sum_{n=1}^{N}\sum_{m=1}^{N;m\neq n}\left[\frac{-1}{r_{nm}}\frac{\partial\phi_{nm}}{\partial r_{nm}}\right](\mathbf{r}_i^{(n)}-\mathbf{r}_i^{(m)})(\mathbf{r}_j^{(n)}-\mathbf{r}_j^{(m)})(V_{\text{simulation}})^{-1}\right.\end{aligned} \tag{T9}$$

$$\begin{aligned}\Pi_{ij}&=-|\mathbf{J}|^{-1}[\delta_{ij}(\tau_{kp}\eta_{kp})+(\mathbf{J}_{ki}^{-1}\tau_{kp}\mathbf{J}_{jp})]\\&=-[\delta_{ij}(\sigma_{kp}\mu_{kp})+(\mathbf{J}_{ki}^{-1}\mathbf{J}_{kp}^{-1}\sigma_{pj})]\end{aligned} \tag{T10}$$

systems, while elsewhere we discuss some advantages of scaled coordinates for the simulation of crystalline materials.[14] All of the equations in Table III have been written in physical rather than virtual time. Nosé[6] and Evans and Holian[25] have discussed the computation of statistical averages using either physical time or virtual time, and Nosé[28] has emphasized that realistic particle dynamics occurs only in physical time, and that a consistent dynamical interpretation only results from consideration of s as a time scale and not a mass scale.[10] While the dynamics of the time scale (T1) does indeed decouple from the remaining equations of motion,[8,27,28] we have retained it for completeness. In addition to the numerical test provided by the conservation of (4.1), Branka and Parrinello[32] have used moments of the time scale to compute differences in free energy.

The numerical value of f can be determined following the standard interpretation of s as a time scale.[6,28] Integration of trajectories in physical time effectively removes one degree of freedom. Imposition of the constraints that there be no center-of-mass motion of the atoms eliminates three additional degrees of freedom; imposition of the dynamical constraint to suppress rigid rotations of the crystal described below removes three more degrees of freedom. We therefore set $f=3N+3$. The results in the equipartition of thermal energy over all degrees of freedom. The time scale can vary greatly from unity when initializing the simulation; we reset the time scale s to unity after such initialization. Also, we rescale the virtual time to the physical time every time a new condition is imposed on the simulation, e.g., every time the pressure is increased.

We now describe the dynamical constraint to eliminate rigid rotations of the crystal. Nosé and Klein[16] analyzed the lack of rotational invariance of Parrinello-Rahman dynamics in detail, and demonstrated that the phase space sampled by the equations of motion was too large in that rigid rotations were included. They imposed a geometrical constraint that required the matrix of lattice vectors to remain symmetric. Another geometric constraint to restrict the matrix of lattice vectors to upper triangular form was suggested by Ciccotti and Ryckaert.[26] By contrast, we present a dynamical constraint on the momenta associated with the cell degrees

TABLE III. Alternative atomic equations of motion. It is understood that the center-of-mass motion has been removed from all equations, and that all the equations have been written in physical time.

(1) Scaled coordinates and momenta:

$$\dot{\mathbf{q}}^{(n)}=\mathbf{g}^{-1}\pi^{(n)}/\mu_n$$
$$\dot{\pi}^{(n)}=\mathbf{g}\tilde{\mathbf{F}}^{(n)}-\xi\pi^{(n)}$$

(2) Scaled coordinates and accelerations:

$$\ddot{\mathbf{q}}^{(n)}=\tilde{\mathbf{F}}^{(n)}/\mu_n-(\omega+\xi)\dot{\mathbf{q}}^{(n)}$$
$$\omega=\mathbf{g}^{-1}[\mathbf{a}^T\dot{\mathbf{a}}+(\mathbf{a}^T\dot{\mathbf{a}})^T]$$

(3) Cartesian coordinates and momenta:

$$\dot{\mathbf{r}}^{(n)}=\mathbf{p}^{(n)}/\mu_n+(\dot{\mathbf{a}}\mathbf{a}^{-1})\mathbf{r}^{(n)}$$
$$\dot{\mathbf{p}}^{(n)}=\bar{\mathbf{F}}^{(n)}-[(\dot{\mathbf{a}}\mathbf{a}^{-1})^T+\xi\mathbf{1}](\mathbf{p}^{(n)})$$

(4) Cartesian coordinates and accelerations:

$$\ddot{\mathbf{r}}^{(n)}=\bar{\mathbf{F}}^{(n)}/\mu_n+\{[\dot{\mathbf{a}}\mathbf{a}^{-1}-(\dot{\mathbf{a}}\mathbf{a}^{-1})^T]-\xi\mathbf{1}\}\dot{\mathbf{r}}^{(n)}$$
$$+\{(\ddot{\mathbf{a}}\mathbf{a}^{-1})-\{[\dot{\mathbf{a}}\mathbf{a}^{-1}-(\dot{\mathbf{a}}\mathbf{a}^{-1})^T]-\xi\mathbf{1}\}\dot{\mathbf{a}}\mathbf{a}^{-1}\}\mathbf{r}^{(n)}$$

The scaled force is

$$\tilde{\mathbf{F}}^{(n)}=\left[\sum_{m=1}^{N;m\neq n}\left[\frac{-1}{r_{nm}}\frac{\partial\phi_{nm}}{\partial r_{nm}}\right](\mathbf{q}^{(n)}-\mathbf{q}^{(m)})\right],$$

and the Cartesian force is:

$$\bar{\mathbf{F}}^{(n)}=\sum_{m=1}^{N;m\neq n}\left[\left[\frac{-1}{r_{nm}}\frac{\partial\phi_{nm}}{\partial r_{nm}}\right](\mathbf{r}^{(n)}-\mathbf{r}^{(n)})\right].$$

of freedom; this allows one a wider choice of lattice vectors, and imposes no symmetries other than those required by elastic theory.

To lowest order, and for a sufficiently small time step λ, the deformation gradient can be integrated as

$$\mathbf{J}_{ij}(t+\lambda)=\mathbf{J}_{ij}(t)+\lambda\Omega_{ij}(t)/W$$
$$=[\delta_{ik}+\lambda\Omega_{in}(t)\mathbf{J}^{-1}_{nk}(t)/W]\mathbf{J}_{kj}(t)\ . \quad (4.5)$$

The infinitesimal strain may then be identified through the relation

$$\mathbf{J}_{ij}(t+\lambda)=[\delta_{ik}+\varepsilon_{ik}(t)]\mathbf{J}_{kj}(t)\ , \quad (4.6)$$

where $\varepsilon_{ij}(t)$ is the infinitesimal strain as computed at time t. The rigid rotations are eliminated through symmetrization of the infinitesimal strain,

$$\bar{\varepsilon}_{ij}(t)=\tfrac{1}{2}[\varepsilon_{ij}(t)+\varepsilon_{ji}(t)]\ ,$$
$$\mathbf{J}_{ij}(t+\lambda)=[\delta_{ik}+\bar{\varepsilon}_{ik}(t)]\mathbf{J}_{kj}(t)\ . \quad (4.7)$$

This is perfectly general as infinitesimal rotations commute, and implies we use the following transformed momentum matrix:

$$\bar{\Omega}_{ij}(t)=\tfrac{1}{2}[\Omega_{im}(t)\mathbf{J}^{-1}_{mk}(t)+\Omega_{km}(t)\mathbf{J}^{-1}_{mi}(t)]\mathbf{J}_{kj}(t)\ . \quad (4.8)$$

The effect of this dynamical constraint is to restrict shearing deformations of the simulation cell to include only pure shears.

One immediate point of concern is the formal lack of symmetry of the effective external pressure,

$$\Pi_{ij}\neq\Pi_{ji}\ . \quad (4.9)$$

Typically, a lack of symmetry of a pressure or stress matrix is associated with rigid rotations of the crystal[12] due to unbalanced torques. At first (4.9) seems counterintuitive because it implies rotation of the crystal even if we specify the stress $\sigma_{ij}=\sigma_{ji}$ to be symmetric. However, the effective external pressure must be asymmetric because the unrestricted phase space of the deformation gradient includes rigid rotations of the crystal. This naturally gives rise to dynamics that include rigid rotations of the crystal, and emphasizes the dynamical nature of the constraint that must be imposed. The algorithm (4.5)–(4.8) is more involved than simply symmetrizing Π_{ij}. However, we have noted that a numerical consequence of suppressing rigid rotations of the crystal as described above is that the effective external pressure is indeed rendered symmetric.

The dynamical balance of $\mathbf{P}_{ij}$ and Π_{ij}, implied by Table II, Eq. (T7), expresses the *nonlinear tensorial virial theorem for elastic media:*

$$\langle\mathbf{P}_{kq}\rangle\approx\langle\Pi_{kq}\rangle\ . \quad (4.10)$$

These equations state that at equilibrium, the internal virial pressure $\mathbf{P}_{ij}$, dynamically balances the effective external pressure Π_{ij}. In contradistinction, the internal virial pressure $\mathbf{P}_{ij}$ balances the negative of the stress σ_{ij} only in the limit of infinitesimal deformations,

$$-\sigma_{ij}=\lim_{\mathbf{J}_{ij}\to\delta_{ij}}[\Pi_{ij}]\ , \quad (4.11)$$

which leads to the linearized virial theorem:

$$\langle\mathbf{P}_{kq}\rangle\approx-\sigma_{kq}\ . \quad (4.12)$$

Here, as the cell deforms, the external pressure remains constant and balances the internal virial pressure dynamically. There is thus no material response of the system (i.e., there is no change in the pressure of the elastic reservoir upon deformation of the simulation cell) nor any memory of the reference lattice when atomistic simulations are formulated using a linear theory.

V. MD AND MC SIMULATIONS OF A MARTENSITIC TRANSFORMATION

MD and MC simulations of a structural phase transformation induced by applied hydrostatic pressure have been performed in order to verify the nonlinear theory presented in the previous sections. An infinite relaxation time is imposed, such as would be the case if relaxation occurred due to the migration of extended defects, etc., whose motion is slow on an atomic time scale. The specific numerical values for cohesive energies, densities,

etc., are of little interest; rather, we seek answers to several qualitative questions: Is the nonlinear tensorial virial theorem in fact obeyed by the MD simulations? Do the MC simulations agree with the MD calculations? How are any geometric differences in the choice of crystalline cells manifested in the results? Is there a signature for the change in symmetry which occurs upon transformation? What new physics do these nonlinear simulations include? Are any deficiencies in the physical description present?

We can compare our MD and MC simulations with previous MD simulations that used the same potential and employed an essentially linear theory.[33] There the equations of motion for the cell dynamics implied that the internal virial pressure dynamically balanced the external pressure as in (4.12) and not the effective external pressure as described by (4.10). A hcp final structure was reported,[33] whereas our results indicate that the fcc structure is favored via the classic Bain strain. The inclusion of nonlinear effects—and in particular, the dependence on history in the formulation—may thus lead to qualitatively different results.

The interatomic interaction used in these simulations is a smooth two-parameter pair potential[33] whose energy and length scales have been chosen to yield the cohesive energy and bcc lattice constant of Fe. We refer to this structure as the bcc ground state, although the close-packed structures possess a lower minimum cohesive energy at higher density. In Fig. 1 are shown graphs of the cohesive energy in eV (i.e., the potential energy per atom) versus the dimensionless density (relative to the bcc ground state) for the bcc, fcc, and hcp structures at zero temperature. That the fcc and hcp structures are nearly degenerate until a high density is reached is a consequence of the potential having a short range and the cohesive energy being dominated by the contributions from the nearest neighbors. The fcc and hcp curves cross the bcc curve only slightly above its minimum; the choice of the energy scale requires that a low absolute temperature be maintained in order for the bcc ground state to remain stable when no pressure is applied. In the $(NT\sigma_{ij})$ simulations that follow, the temperature of the thermal reservoir is $T=100$ K. It goes without saying that this material on the computer bears little resemblance to Fe in the laboratory, but it provides dramatic numerical confirmation of the theory we have presented.

After a suitable equilibration period under zero external pressure, each nonlinear MD and MC simulation was subjected to a series of discrete increases in the applied hydrostatic pressure $-\sigma_{ij}=P_{\text{external}}\delta_{ij}$. Having chosen length, time, and energy to be computed in Å, ps, and eV, respectively, the pressure is given in units of eV Å^{-3}; we have not converted to Pa for these model calculations. Similarly, the internal mass unit was chosen so that the expression (mass)×(velocity)^2, where velocity has units of Å ps^{-1}, yields an expression for energy in eV; the multi-

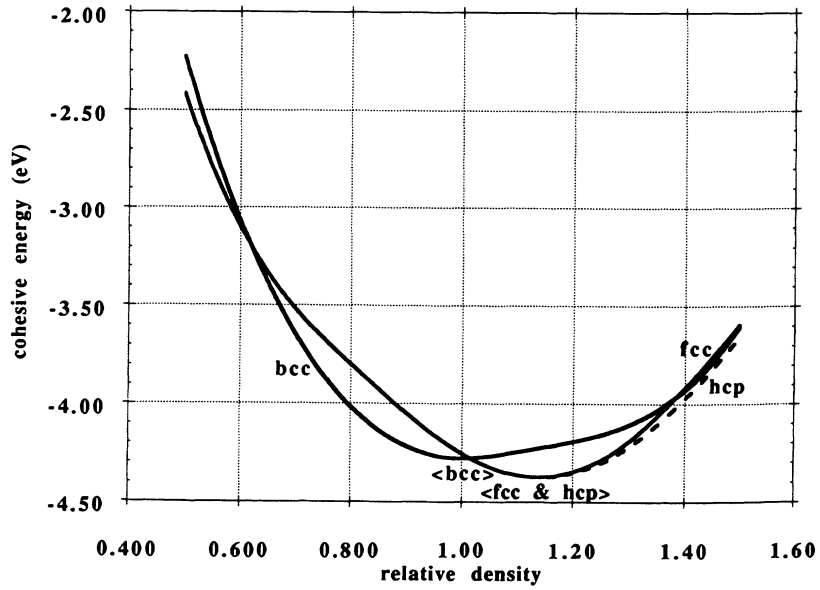

FIG. 1. Cohesive energy vs relative density for bcc, fcc, and hcp crystals. The three curves show the cohesive energy in eV of the bcc, fcc, and hcp structures as a function of the dimensionless density, relative to the bcc ground state. Compare this graph with Fig. 10 from Ref. 33; the differences in energy and length scales do not affect the basic physics of the problem. The general functional form of the pair potential is $\phi\{r_{nm}\}=\varepsilon[\bar{r}^{-p}-\bar{r}^{-q}]\exp[(\bar{r}-\bar{r}_0)^{-1}]$, for $\bar{r}<\bar{r}_0$, and $\phi\{r_{nm}\}=0$, for $\bar{r}\geq\bar{r}_0$, where $\bar{r}=r_{nm}/\sigma$. The potential and all its derivatives vanish at $\bar{r}=\bar{r}_0$. This smoothness, in addition to its flexibility and simplicity, account for the computational convenience of the potential. The form is due to Stillinger and Weber (Ref. 34). The energy and length scales used in the simulations reported here are $\varepsilon=2.065\,777\,3$ eV and $\sigma=2.129\,786$ Å, respectively. The other dimensionless parameters are $p=12$, $q=-1$, and $\bar{r}_0=2$. The cutoff length used in the simulations is thus $r_{\text{cut}}=\sigma\bar{r}_0\approx 4.5$ Å. With these parameters, the bcc ground state is specified by the lattice constant 2.8665 Å and cohesive energy −4.28 eV.

plicative factor that converts atomic mass units (amu) to our internal mass units (imu) is $1.036471\,5\times10^{-4}$. A range of the effective masses Q and W were examined, and the results were found to be insensitive as long as the masses were not so large as to decouple the atomic and scaling degrees of freedom nor so small as to cause numerical instability in the integration. The MD trajectories were obtained with $Q=8617\,068\,4\times10^{-3}$ eV ps^2, and $W=6.387\,376\,6\times10^{-3}$ imu Å^2.

The final atomic configurations of the trajectories were analyzed in the following manner. A computer-generated picture of each final atomic configuration was rotated until the hexagonal close-packed planes were superimposed upon one another; the camera angle of this picture was then rotated 90°, and then further rotated about the normal to the close-packed planes until the atoms became superimposed again. The stacking of the close packed planes could then be observed. The (*ABCABCABC*. . .)

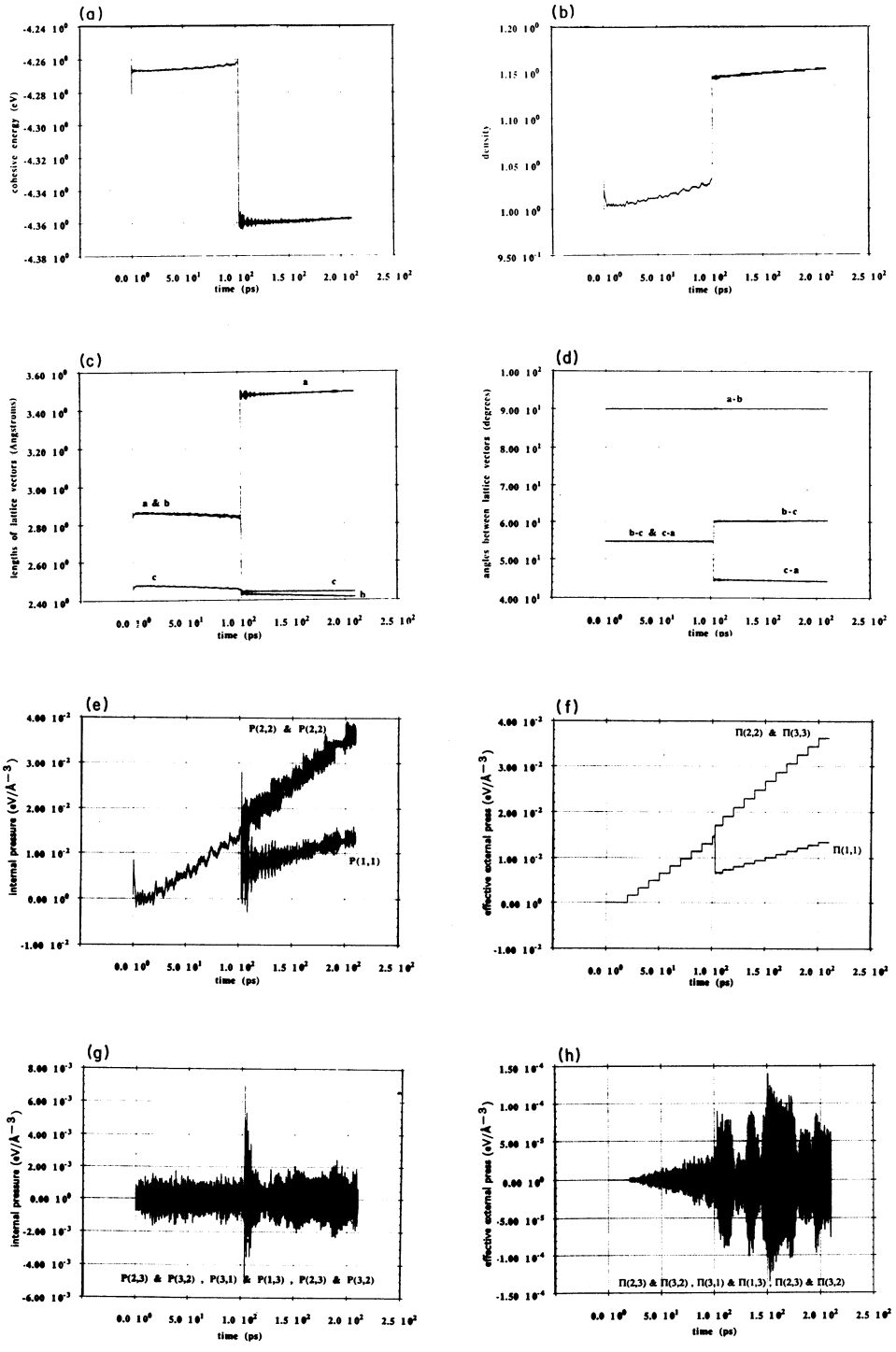

FIG. 2. Trajectories for the MD simulation whose skewed initial volume contained 1728 atoms: (a), the cohesive energy; (b), the relative density; (c), the lengths of the lattice vectors; (d), the angles between the lattice vectors; (e), the diagonal matrix elements of the internal virial pressure; (f), the diagonal matrix elements of effective external pressure; (g), the off-diagonal matrix elements of the internal virial pressure; (h), the off-diagonal matrix elements of the effective external pressure.

pattern characteristic of the fcc structure was observed in every simulation, rather than the ($ABABAB\ldots$) pattern of the hcp structure. The trajectories summarized in Figs. 2–5 represent simulation volumes having different initial shapes, a skewed cell having 1728 atoms and a cubic cell having 432. The lattice vectors ($\mathbf{b}_{ij}$) and basis vectors ($\boldsymbol{\beta}_{ij}$) used to describe the initial bcc lattice are given in Table IV.

First, comparisons of the cohesive energy (a) and density (b) for Figs. 2–5 reveal the same clear, sharp structural transformation; the final densities and cohesive energies are the same, as is the density at which the transformation commences. Second, comparison of the lengths of the lattice vectors (c) and the angles between the lattice vectors (d) for the MD and MC simulations demonstrate that the MD and MC simulations describe the same physical mechanisms for the macroscopic deformation of the cell. Comparison of the geometrical variables (c) and (d) for trajectories having different initial geometries show distinct macroscopic pathways for the deforma-

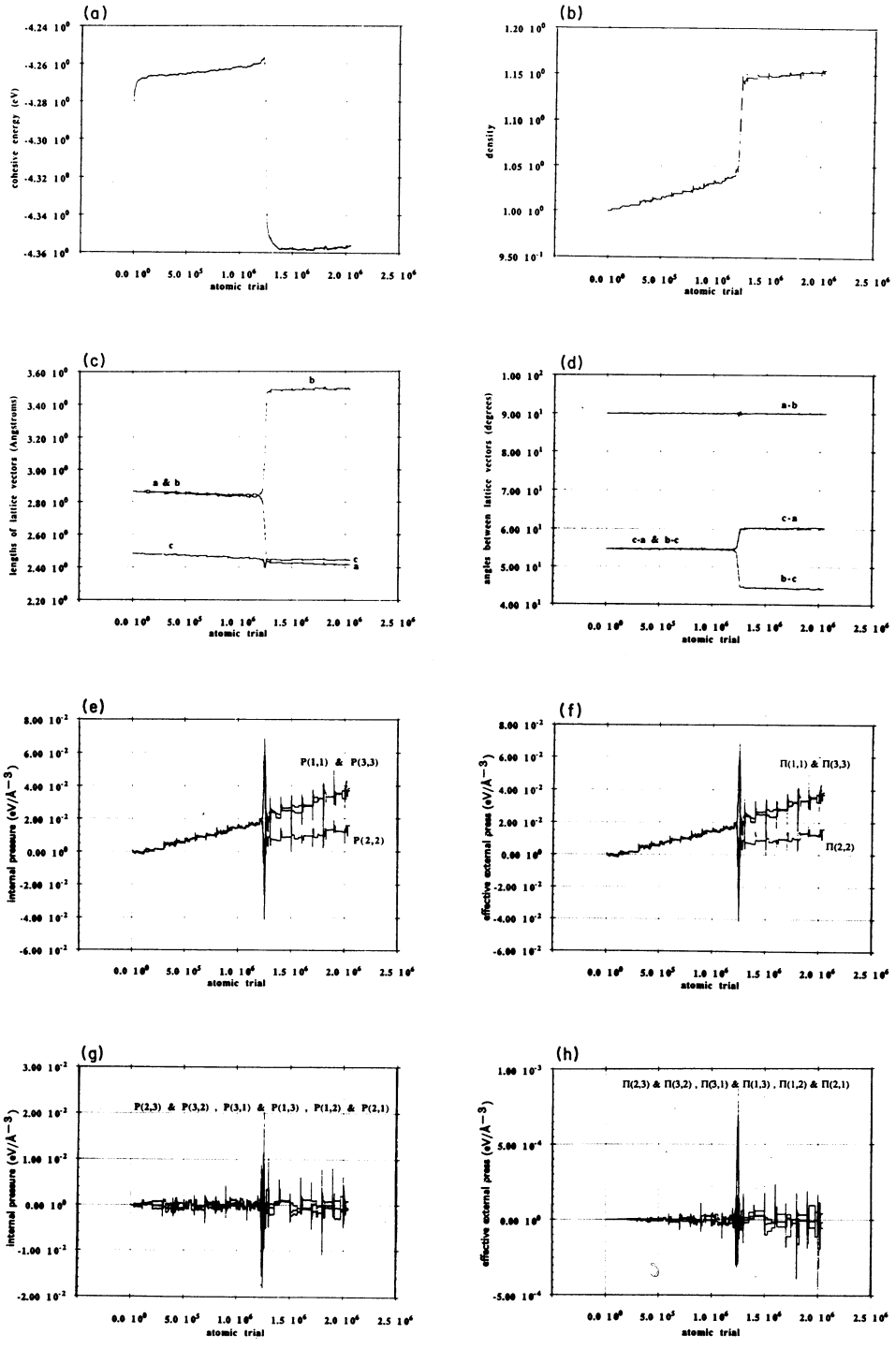

FIG. 3. Trajectories for the MC simulation whose skewed initial volume contained 1728 atoms; (a)–(h) as in Fig. 2.

tions. Figures 4 and 5 represent explicitly the classic "Bain" deformation.

Third, the trajectories for the diagonal elements of the internal (e) and effective external (f) pressure tensor and the off-diagonal elements of the internal (g) and effective external (h) pressure tensor for simulations having the same initial geometries demonstrate that the elements of the internal virial pressure fluctuate about the corresponding elements of the effective external pressure. The MD and MC simulations therefore consistently satisfy the nonlinear tensorial virial theorem throughout the structural transformation in each case. The MD equations of motion guarantee this dynamical balance, but no driving term is used in the MC simulations to insure this result. Further, the symmetry of the effective external pressure tensor is clearly seen in each case.

Fourth, the diagonal elements of the internal (e) and effective external (f) pressure tensor and the off-diagonal elements of the internal (g) and effective external (h) pressure tensor depart from hydrostatic behavior upon the

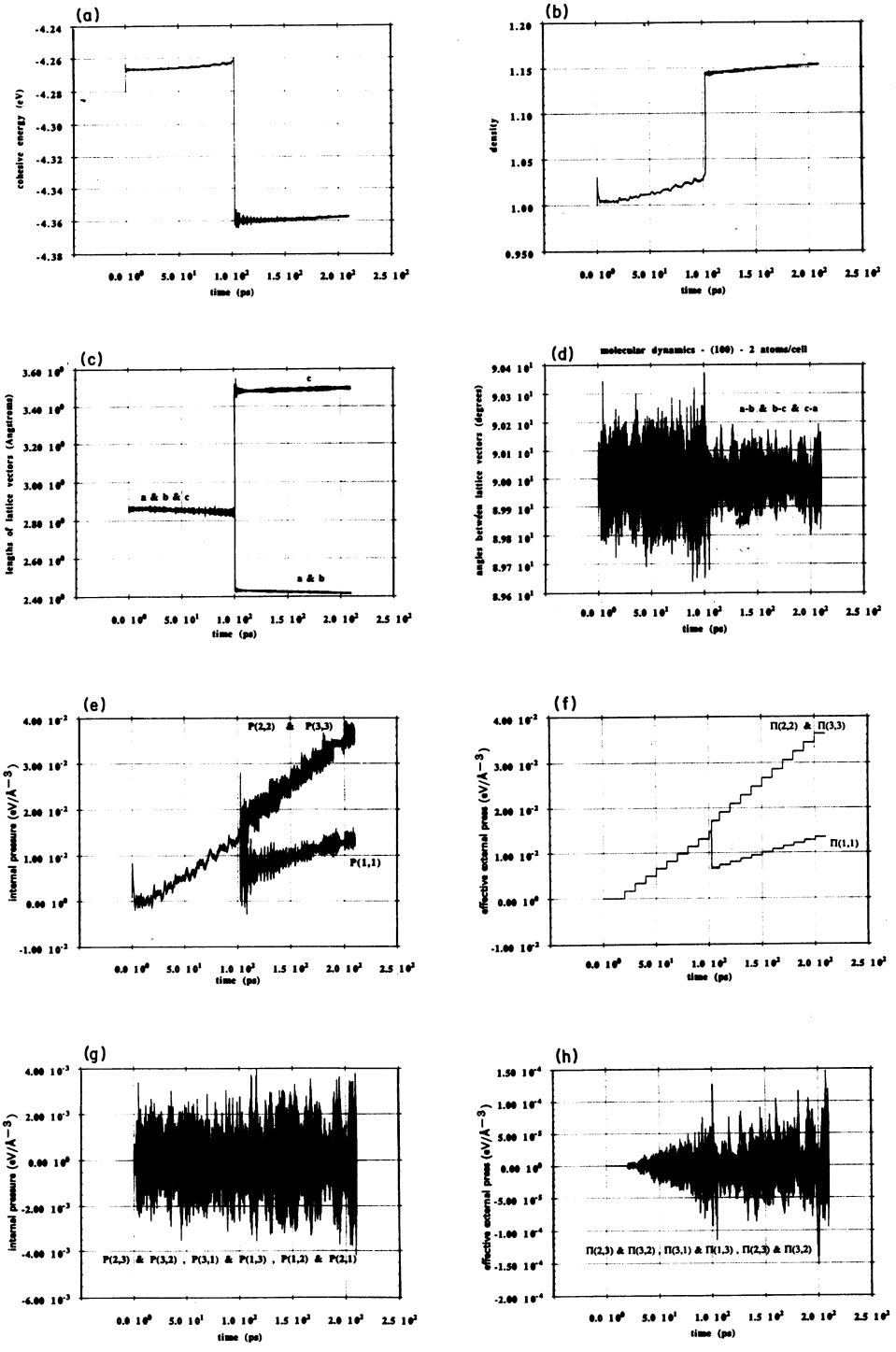

FIG. 4. Trajectories for the MD simulation whose cubic initial volume contained 432 atoms; (a)–(h) as in Fig. 2.

structural phase transformation, due to the mismatch between the dynamic lattice and the (static) reference lattice. This is clearly consistent with the interpretation of the lattice vectors $\mathbf{a}_{ij}$ as describing a macroscopic inclusion of the new phase within the parent crystal described by $\mathbf{b}_{ij}$. The mismatch between $\mathbf{a}_{ij}$ and $\mathbf{b}_{ij}$ is modeled at the continuum level; no atomistic description of any interface between the old and new phases is present. The mismatch of the old and new lattices results in there being a strain energy carried by the elastic field at the end of the calculation, and this strain depends upon the shape of the inclusion of new phase. (Similar simulations not reported here demonstrate an orientational dependence as well.) No mechanism for relaxing this final stress is present in these simulations. Allowance for stress relaxation on some finite time scale would result in the eventual coalescence of the diagonal elements of the stress tensors, and the off-diagonal elements would re-

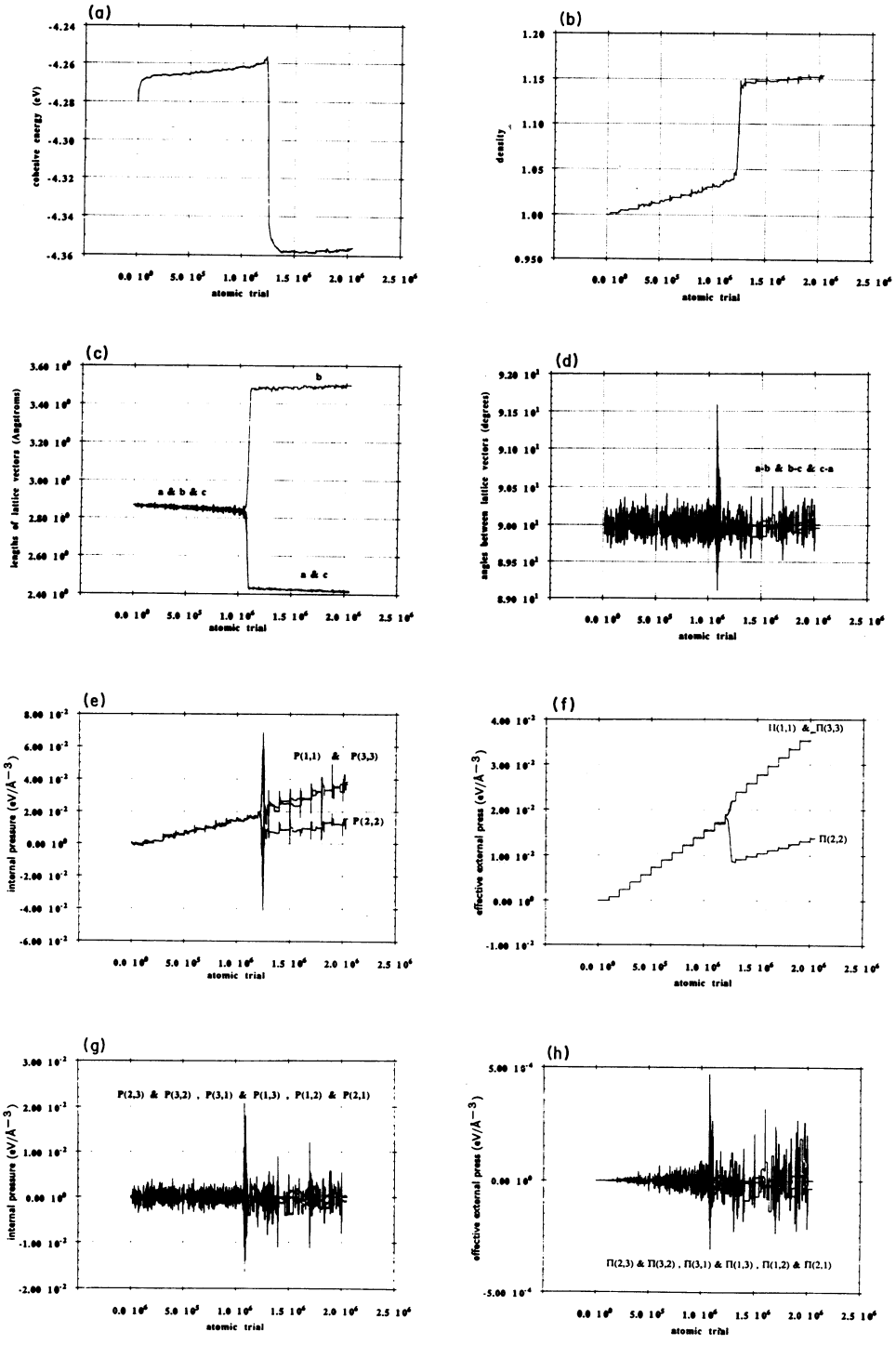

FIG. 5. Trajectories for the MC simulation whose cubic initial volume contained 432 atoms; (a)–(h) as in Fig. 2.

TABLE IV. Initial bcc lattice and basis vectors.

(100) face normal to z axis, and one atom per crystalline cell:

$$\mathbf{b}_{ij}=\begin{bmatrix}2.8665 & 0.0000 & 1.4333\\ 0.0000 & 2.8665 & 1.4333\\ 0.0000 & 0.0000 & 1.4333\end{bmatrix},\quad \beta_{ij}=\begin{bmatrix}0.000\\ 0.0000\\ 0.0000\end{bmatrix}$$

Volume of crystalline cell: $|\mathbf{b}|=11.776\,76$ Å^3

Number of atoms in simulation volume: $N=1728$

(100) face normal to z axis, and two atoms per crystalline cell:

$$\mathbf{b}_{ij}=\begin{bmatrix}2.8665 & 0.0000 & 0.0000\\ 0.0000 & 2.8665 & 0.0000\\ 0.0000 & 0.0000 & 2.8665\end{bmatrix},\quad \beta_{ij}=\begin{bmatrix}0.0000 & 1.4333\\ 0.0000 & 1.4333\\ 0.0000 & 1.4333\end{bmatrix}$$

Volume of crystalline cell: $|\mathbf{b}|=23.553\,52$ Å^3

Number of atoms in simulation volume: $N=432$

turn to zero. However, even rapid stress relaxation on a laboratory time scale can sometimes be slow on an atomic time scale, and the qualitative effects displayed here would nonetheless be present until the system relaxed. These transformations are not reversed by decreasing the applied pressure $(-\sigma_{ij})$ to zero; the crystals remain stuck in the close-packed structure having the lower cohesive energy when the applied stress σ_{ij} is reduced to zero.

In the slow-relaxation limit, the splitting of these pressure fields serves as a dramatic signature of the symmetry breaking that accompanies a phase transformation; in this case, the initially isotropic pressure field is rendered anisotropic. Initially in each simulation, the diagonal elements of the internal virial and effective external pressures fluctuate about the same values as $(-\sigma_{ij})$ is increased; the off-diagonal elements of the pressure matrices fluctuate about zero. When the structural transformation occurs, the diagonal elements of the internal virial and effective external pressure fields split into separate branches while maintaining the dynamical balance (4.10), and this splitting becomes more pronounced as $(-\sigma_{ij})$ is increased. Similarly, the off-diagonal elements sometimes split into separate branches while dynamically maintaining symmetry and (4.10). Again, however, the nonlinear tensorial virial theorem is obeyed throughout the transformation. Further, the imposition of our dynamical constraint to remove rigid rotations from the simulation has the numerical effect of rendering the effective external pressure Hermitian. Because the pressure before the transformation is isotropic, which elements of the pressures follow which branches after the transformation is purely a matter of chance; that is, we can effect a reordering of the elements of the final pressure matrices by changing the seed on the random-number generator that determines the initial thermal velocities in the MD algorithm, or that determines the acceptance or rejection of Metropolis moves in the MC algorithm. These differences in ordering can appear in MD and MC trajectories starting from the same initial atomic configuration; the corresponding simulations describe the same physical transformation to the same final atomic structure within inclusions having different shapes and different orientations with respect to the parent crystal.

VI. DISCUSSION

These simulations appear counterintuitive because of the interpretation of σ_{ij} as the stress that would be in the crystal in the absence of any deformation, yet we are considering an isothermal-isostress ensemble. One is accustomed to think of the stress that specifies the ensemble as being imposed throughout the system at equilibrium. However, the nonlinearity in the problem prevents one from knowing the equilibrium stress before it is imposed. Further insight into this problem can be gained from considering the $V(dP)$-type work required to change the pressure in the crystal from the effective external pressure Π_{ij} to $(-\sigma_{ij})$. A simple calculation yields

$$\begin{aligned}&V_{\text{simulation}}(-\sigma_{kk}-\Pi_{kk})\\ &\quad=V_{\text{simulation}}\{[-\sigma_{kk}+(\mathbf{J}_{pk}^{-1}\mathbf{J}_{ph}^{-1}\sigma_{hk})]+3\sigma_{kp}\mu_{pk}\}\\ &\quad=V_{\text{simulation}}(\sigma_{kp}\mu_{pk})=\Phi_{\text{strain}}\ .\end{aligned}\tag{6.1}$$

Thus the difference between Π_{ij} and $(-\sigma_{ij})$ can be ascribed to the atomistic system having done work on the continuum elastic reservoir and/or vice versa. We emphasize that this physically appealing result is guaranteed by satisfaction of the nonlinear tensorial virial theorem.

The difference between Π_{ij} and $(-\sigma_{ij})$ and the splitting of the pressure fields arises from certain memory effects which arise in the present analysis from the inclusion of the new phase in the strain field of the parent crystal. Before the phase transformation, as $(-\sigma_{kq})=P_{\text{external}}\delta_{kq}$ is increased, the crystal is subjected to a series of infinitesimal deformations and the isotropy of the pressure fields is maintained. The diagonal elements of the internal virial and effective external pressures all fluctuate about the same values, while the off-diagonal elements of these matrices fluctuate about zero. When the crystal undergoes a large and rapid deformation during the structural transformation, the symmetry of the lattice changes. However, the elastic reservoir does not undergo a corresponding transformation; it retains a memory of the crystal's initial shape. The accommodation of this deformed crystal within the elastic reservoir having a complete memory of the original lattice thus gives rise to the anisotropic pressures that are manifested by the splitting of the pressure fields. This is a physical effect that occurs when a new structural phase is incorporated into the parent crystal[22] in the absence of any rapid mechanism for stress relaxation.

Furthermore, the arbitrary choice of the crystalline cell whose vectors scale the atomic coordinates and momenta determines the shape of the inclusion of the new phase. While the MD equations are formally invariant to modular transformations, it must be remembered that such transformations involve both the dynamic and reference lattices. The simulations involve only a deformation of the dynamic lattices and, as indicated by the results, the strain induced in the parent crystal does depend on the

shape of the inclusion as dictated in these simulations by the choice of initial lattice vectors. This again is observed experimentally, where the effects of such strains are believed to be important in determining the pattern of growth of the new phase within the parent crystal.[22] This history dependence arises naturally within the nonlinear framework we have presented.

One obvious extension of the present theory would be to allow the elastic reservoir to relax to the new configuration. This is in accordance with the principle of fading memory;[21] this simply states that one does not have to know the entire history of a crystal from the time of creation in order to describe its current state. The strain present at the end of the simulations described here must relax on some time scale, and in particular the diagonal elements must collapse to balance the imposed hydrostatic pressure eventually. These arguments pertain to the construction of a *constitutive equation* for the material, in effect an equation of state which explicitly includes dissipative effects. This implies adopting an explicitly nonequilibrium treatment which will be developed in a further publication.

ACKNOWLEDGMENTS

We wish to thank Mario Ancona of the Electronics Science and Technology Division at NRL for his careful reading of drafts of this article and for his insightful comments. We also wish to thank Renata M. Wentzcovitch and Mo Li for many useful discussions. We thank Rob Rosenberg, Jeannie Osburn, and Chas. Williams of the Research Computation Division at NRL for assistance in performing the calculations.

[1]Hans C. Andersen, J. Chem. Phys. **72**, 2384 (1980).
[2]M. Parrinello and A. Rahman, Phys. Rev. Lett. **45**, 1196 (1980).
[3]M. Parrinello and A. Rahman, J. Appl. Phys. **52**, 7182 (1981).
[4]M. Parrinello and A. Rahman, J. Chem. Phys. **76**, 2662 (1982).
[5]Shuichi Nosé, Mol. Phys. **52**, 255 (1984).
[6]Shuichi Nosé, J. Chem. Phys. **81**, 511 (1984).
[7]Shuichi Nosé, Mol. Phys. **57**, 187 (1986).
[8]William G. Hoover, Phys. Rev. A **31**, 1695 (1985); **34**, 2499 (1986).
[9]John R. Ray and Aneesur Rahman, J. Chem. Phys. **80**, 4423 (1984).
[10]John R. Ray and Aneesur Rahman, J. Chem. Phys. **82**, 4243 (1985).
[11]John R. Ray, J. Chem. Phys. **79**, 5128 (1983).
[12]R. N. Thurston, in *Physical Acoustics: Principles and Methods,* edited by Warren P. Mason (Academic, New York, 1964), pp. 1–110.
[13]J. V. Lill and Jeremy Q. Broughton, Phys. Rev. B **46**, 12 068 (1992); **48**, 3580 (1993).
[14]J. V. Lill, Comput. Phys. Commun. (to be published).
[15]Guilhem Marc and W. G. McMillan, in *Advances in Chemical Physics,* edited by I. Prigogine and Stuart A. Rice (Wiley, New York, 1985), Vol. LVIII, pp. 209–361. See section II.A.5 for the tensorial extension of the virial theorem.
[16]Shuichi Nosé and M. L. Klein, Mol. Phys. Rev. **50**, 1055 (1983).
[17]Charles L. Cleveland, J. Chem. Phys. **89**, 4987 (1988).
[18]Renata M. Wentzcovitch, Phys. Rev. B **44**, 2358 (1991).
[19]Nicholas Metropolis, Arinna W. Rosenbluth, Marshall N. Rosenbluth, Augusta H. Teller, and Edward Teller, J. Chem. Phys. **21**, 1087 (1953).
[20]Max Born and Ken Huang, *Dynamical Theory of Crystal Lattices* (Clarendon, Oxford, 1954).
[21]C. Truesdell and W. Noll, in *Encyclopedia of Physics,* edited by S. Flügge (Springer-Verlag, Berlin, 1965), Vol. III/3. See Sec. 19A for a discussion of the principle of material-frame indifference. See Secs. 38 and 39 for discussions of the principle of fading memory and stress relaxation.
[22]A. G. Khachaturyan, *Theory of Structural Transformations in Solids* (Wiley, New York, 1983). See Chap. 7 for a discussion of the elastic strain induced in the parent crystal by inclusion of the daughter phase. Chapter 1 contains a discussion of crystal symmetry, including primitive and unit cells. Martensitic transformations are described in Chap. 6.
[23]I. R. McDonald, Mol. Phys. **23**, 41 (1972).
[24]Robin L. Blumberg Silinger, Zhen-Gang Wang, and William M. Gelbart, J. Chem. Phys. **95**, 9128 (1991).
[25]Denis J. Evans and Brad Lee Holian, J. Chem. Phys. **83**, 4069 (1985).
[26]G. Ciccotti and J. P. Ryckaert, Comput. Phys. Rep. **4**, 345 (1986).
[27]Simone Melchionna, Giovanni Ciccotti, and Brad Lee Holian, Mol. Phys. **78**, 533 (1993).
[28]Shuichi Nosé, Prog. Theor. Phys. Suppl. **103**, 1 (1991).
[29]Aurel Bulgac and Dimitri Kusnezov, Phys. Rev. A **42**, 5045 (1990).
[30]Dimitri Kusnezov, Aurel Bulgac, and Wolfgang Bauer, Ann. Phys. (Leipzig) **204**, 155 (1990).
[31]D. M. Bylander and Leonard Kleinman, Phys. Rev. B **46**, 13 756 (1992).
[32]A. Branka and M. Parrinello, Mol. Phys. **58**, 989 (1986).
[33]Kar Yue Lee and John R. Ray, Phys. Rev. B **39**, 565 (1989).
[34]Frank H. Stillinger and Thomas A. Weber, Phys. Rev. A **28**, 2408 (1983).